Inversion of airborne geophysics over the DO-27/DO-18 kimberlites — Part 2: Electromagnetics

Dominique Fournier[1], Seogi Kang[1], Michael S. McMillan[1], and Douglas W. Oldenburg[1]

Abstract

We focus on the task of finding a 3D conductivity structure for the DO-18 and DO-27 kimberlites, historically known as the Tli Kwi Cho (TKC) kimberlite complex in the Northwest Territories, Canada. Two airborne electromagnetic (EM) surveys are analyzed: a frequency-domain DIGHEM and a time-domain VTEM survey. Airborne time-domain data at TKC are particularly challenging because of the negative values that exist even at the earliest time channels. Heretofore, such data have not been inverted in three dimensions. In our analysis, we start by inverting frequency-domain data and positive VTEM data with a laterally constrained 1D inversion. This is important for assessing the noise levels associated with the data and for estimating the general conductivity structure. The analysis is then extended to a 3D inversion with our most recent optimized and parallelized inversion codes. We first address the issue about whether the conductivity anomaly is due to a shallow flat-lying conductor (associated with the lake bottom) or a vertical conductive pipe; we conclude that it is the latter. Both data sets are then cooperatively inverted to obtain a consistent 3D conductivity model for TKC that can be used for geologic interpretation. The conductivity model is then jointly interpreted with the density and magnetic susceptibility models from a previous paper. The addition of conductivity enriches the interpretation made with the potential fields in characterizing several distinct petrophysical kimberlite units. The final conductivity model also helps better define the lateral extent and upper boundary of the kimberlite pipes. This conductivity model is a crucial component of the follow-up paper in which our colleagues invert the airborne EM data to recover the time-dependent chargeability that further advances our geologic interpretation.

Introduction

The Tli Kwi Cho (TKC) kimberlite complex, located 28 km southeast of the Diavik Diamond Mine, was identified from an airborne magnetic and frequency-domain electromagnetic (EM) DIGHEM survey in 1992 (Figure 1). The initial discovery targeted two anomalies called DO-18 and DO-27. In Devriese et al. (2017), the first in the three-part series on this area, our colleagues present the background history concerning the discovery and exploration of the region and the inversion and interpretation of the potential field data. The recovered 3D density and magnetic susceptibility models were shown to be extremely valuable in defining the overall structural extent of the pipes and provided a case for defining at least three different kimberlite rock units. In this paper, we focus upon a third physical property, electrical conductivity.

A common geophysical fingerprint for a kimberlite pipe near the poles is a circular strong magnetic anomaly, with a gravitational low and an anomalous EM response. The main rock types found in the Lac de Gras region are summarized in Table 1 and are depicted in Figure 2. Electrical conductivity is relevant to understanding the geology of kimberlites through a few routes. First, many kimberlite pipes are infilled with olivine-rich volcaniclastic sediments (Masun, 1999) and are generally serpentinized through low-temperature metamorphism. Further weathering in the upper region of the kimberlite pipes alters the rocks to the clay minerals that are conductive compared with the host Archean granitic rocks. Second, glacial scouring of the low competency kimberlitic rocks often results in the thick accumulation of glacial tills and lake sediments, which are typically conductive. Both processes can give rise to strong EM anomalies and differentiating between the shallow sediments and the deeper pipe is a key challenge in diamond exploration (Power and Hildes, 2007).

Various geophysical techniques were used during the discovery phase of TKC, but little could be done at the time to model the deposits prior to drilling. It was not until later, after the development of inversion algorithms, that the airborne geophysics would be used to better understand the geometry of the deposit.

No geophysical inversions were attempted until the work of Jansen and Doyle (1998) who use frequency-

[1]University of British Columbia, UBC-Geophysical Inversion Facility, Department of Earth, Ocean, and Atmospheric Sciences, Vancouver, Canada. E-mail: dfournie@eos.ubc.ca; skang@eos.ubc.ca; mmcmilla@eos.ubc.ca; doug@eos.ubc.ca.

Manuscript received by the Editor 8 September 2016; revised manuscript received 24 December 2016; published online 7 June 2017. This paper appears in *Interpretation*, Vol. 5, No. 3 (August 2017); p. T397–T409, 16 FIGS., 5 TABLES.

http://dx.doi.org/10.1190/INT-2016-0140.1.

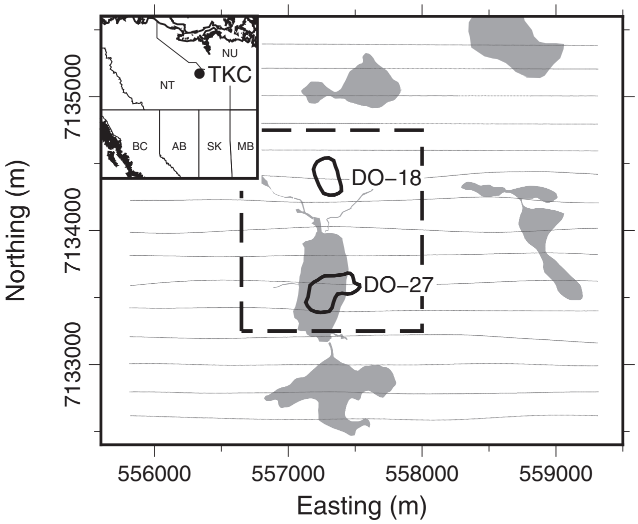

Figure 1. Location map for the DO-18 and DO-27 (TKC) kimberlite deposits, Northwest Territories. DIGHEM survey lines (black) and hydrography (gray) are shown for reference.

Table 1. Expected physical property contrast for kimberlite deposits in the Lac de Gras region.

Rock type	Density	Susceptibility	Conductivity[2]
Glacial till	Moderate	None	Moderate-high
Host rock	Moderate	None	Low
HK	Low-moderate	High	Low-moderate
VK	Low	Low-moderate	Moderate-high
PK	Low	Low-moderate	Moderate-high

[2]The conductivity properties presented herein do not take into account the ice content and temperature of the rocks. As shown by Grimm and Stillman (2015), temperature and ice can significantly change the bulk resistivity of rocks, which can vary seasonally.

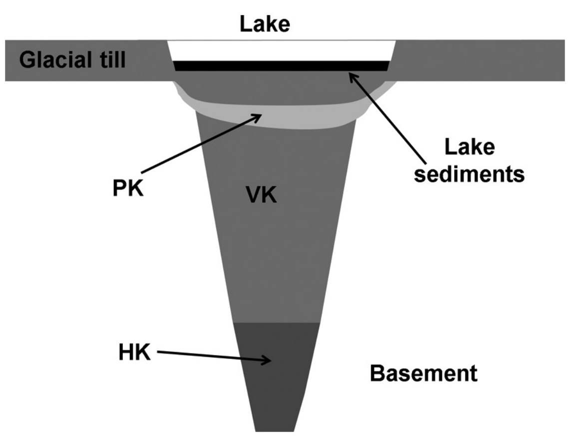

Figure 2. Schematic representation of the kimberlite pipe found in the Lac de Gras region. A lake may be present after glaciation.

domain EM (FEM) Aerodat data and a ground time-domain EM (TEM) NanoTEM survey. One-dimensional conductivity models at DO-27 showed a flat-lying conductor at approximately 50 m depth. Although the depth would suggest a response from the fine-grained glaciofluvial sediments, they interpret the EM anomaly to originate from the clay-bearing minerals within the pipe itself. They hypothesize that the EM systems did not have enough depth penetration to see the deeper part of the pipe.

In a separate analysis involving a VTEM and DIGHEM survey, Witherly (2005) also comes to the same conclusion. The 1D inversion of both data sets seems to indicate a deeper source than the lake sediments, but the vertical location of the recovered conductor remained ambiguous.

In this paper, we investigate the usefulness of airborne EM methods in characterizing the geometry of the kimberlite pipes at TKC. We begin by using our 1D laterally constrained inversions (LCIs) to estimate an approximate large-scale conductivity for the area. This also provides insight into data noise levels. We next address the issue of whether the high conductivity associated with the two pipes is likely due to the near-surface till and sediments (the usual assumption) or whether a significant contribution arises from the pyroclastic units below. For this, we concentrate upon DO-27.

Each EM data set senses the earth differently and has its own issues with respect to experimental noise, and yet, all data are governed by the same physics responding to a common earth. Therefore, our main goal is to find a single conductivity structure that adequately explains all data sets. Recent advancements in meshing, optimization, parallelization, and cooperative/joint inversion of EM codes (Haber and Schwarzbach, 2014; McMillan and Oldenburg, 2014; Yang and Oldenburg, 2014) allow us to invert large-scale airborne EM data sets in an efficient manner. The FEM and TEM data are inverted separately and then cooperatively in three dimensions to obtain the best estimate for a common conductivity model. We use this model in many ways. First, the distribution of conductivity, by itself, allows us to make some geologic inferences about the kimberlites. The model is then analyzed jointly with the density and magnetic susceptibility models from Devriese et al. (2017) to refine our geologic rock model for TKC. Finally, the conductivity model, which is crucial for any estimation of induced polarization (IP) parameters of the rock units, is made available for Kang et al. (2017) of our research.

FEM data

The TKC deposits were primarily a geophysical discovery from a DIGHEM survey flown in 1992 (Jansen and Doyle, 1998). This FEM system has extensively been used in diamond exploration because it operates on a broad range of frequencies to energize conductors at different depths. Three frequencies (900, 7200, and 56,000 Hz) are measured using a horizontal coplanar (HCP) transmitter-receiver configuration, as well as two frequencies (900 and 5000 Hz) measured on a vertical coaxial (VCA) configuration. The highest frequencies can be used to delineate near-surface conductors, whereas deeper structures can potentially be detected at the lower frequencies. As observed on the 56,000 Hz channel (Figure 3a), DO-18 and DO-27 give rise to a strong quadrature component consistent with the early model of two conductive bodies hosted in a resistive granite background (Jansen and Doyle, 1998). The quadrature component correlates well with the hydrography, agreeing with a shallow response from the lake bottom sediments and the glacial till layer. Two elongated and narrow negative anomalies appear in the in-phase maps of the 900 and 7200 Hz (Figure 3b and 3c). These features are associated with intrusive dike swarms known to be the strong magnetic susceptibility anomalies. Both frequencies also highlight well the two pipes in their respective quadrature components (Table 2).

1D inversion

Even though valuable information can be deduced by visual interpretation of the EM data, specific questions regarding the shape and extent of geologic units require the data to be inverted. Early interpretation work done on the FEM data suggested a shallow response from the upper region of the pipe. We first attempt to reproduce the analysis of Jansen and Doyle (1998) in one dimension. The 1D inversion assumes only vertical variations in conductivity, which greatly reduces the complexity and computational cost compared with a full 3D inversion. It can provide a first-order estimate for the background conductivity and a spatial distribution of EM anomalies. It is also a simple and useful processing step to validate the positioning, normalization, and noise level associated with the data. We design a laterally constrained 1D inversion procedure to get a more consistent conductivity distribution in preparation for the full 3D inversion. More details regarding the algorithm are provided in Appendix A. Each 1D inversion is used to populate a large 3D mesh. Variable uncertainty floors are assigned to each frequency to balance their respective contributions. Table 3 summarizes the inversion parameters. We only use the HCP configuration in our work because the VCA data show large variations from line to line and no VCA quadrature component was provided.

Figure 4 presents the recovered conductivity model from the laterally constrained 1D inversion. Both kimberlite pipes are clearly visible on the horizontal section. Conductivity structures seem to be mainly restricted to the upper 200 m below the topography and hosted in a resistive background representative of the old Archean granitic background rocks (20 kΩm). Flat-top conductors are observed at the location of both pipes; however, the broader DO-27 signature extends to a greater depth. The horizontal conductor near DO-18 seems to arc down in cross section, likely due to the 1D representation of a compact 3D object. There is also an indication of a deeper conductor associated with DO-18, but it is substantially weaker than that at DO-27. Overall, this model is consistent with the result obtained by Jansen and Doyle (1998) and shows a thin conductor at the depth of 50 m with the potential for a larger anomaly at depth.

Differentiating between the glaciofluvial sediments and the kimberlite pipe itself is a common problem in diamond exploration in northern Canada (Power and Hildes, 2007). The lack of near-surface conductors recovered away from the kimberlite pipes, however, suggests that the EM response attributed to the till layer may be negligible in this case. We synthetically tested the resolving capabilities of the 1D code (not shown here) with data generated from a compact conductor placed 100 m below the surface. Using identical configurations, the synthetic inversion yielded a similar layered anomaly, which suggests that the flat conductor obtained over DO-18 may be the result of 1D artifacts, and it may not necessarily representative of a true conductive pipe. To fully answer this question, a 3D analysis of the FEM data is required.

3D inversion

Although the 1D inversion of the FEM data yielded valuable information, the geometry of the TKC deposits is clearly 3D, and hence a more sophisticated inversion algorithm is required. The 3D inversion of large FEM data is computationally challenging for many reasons. We have many sounding locations over a large area, and the small transmitter-receiver loop separation requires a small cell size; this results in a prohibitively large mesh for conventional inversion codes. The computational cost can be reduced by the method proposed by Yang and Oldenburg (2014) by subdividing the volume into locally optimized meshes, reducing the size of individual inverse problems. We use a tiled version of e3D-octree

Table 2. Specifications of three different airborne EM systems.

Specs	DIGHEM	VTEM	AeroTEM
Type	Frequency	Time	Time
Waveform	Sinusoidal	Trapezoidal	Triangular
t or f range	900–56 kHz	90–6340 μs	26–1393 μs
t or f channels	10	27 off-time	16 off-time
Geometry	HCP, VCA	HCP	HCP
Offset	8 or 5 m	0 m	0 m
Bird height	30 m	28 m	28 m
Year	1992	2004	2003
Data type	Bz or Bx	dBz/dt	dBz/dt, dBy/dt
Data unit	ppm	pV/A m^4	nT/s

code, an inversion algorithm adapted from Haber and Schwarzbach (2014).

A total of 216 soundings, each consisting of three HCP frequencies were inverted over the deposits. Figure 5 presents sections through the recovered conductivity model. Both pipes show up as discrete and compact conductors extending vertically at depth. The conductivity structure associated with DO-18 appears to be close to the surface, and the pipe is approximately 150 m in diameter. The upper limit of DO-27 is between 20 and 50 m below the lake; this is roughly the known thickness of the till and lake bottom sediments (Eggleston and Brisebois, 2008). Even though this upper limit seems to be well-defined by the inversion, the deeper limits of the pipe remain unclear. The bulk of the low resistivity (<100 Ωm) extends, at most, to 100 m below the till, and the resistivity values gradually increase below that. This may be a consequence of lack of resolving power by the survey. Our result does not exclude the possibility for a deeply rooted conductive pipe, for which the FEM is poorly sensitive, as hypothesized by Jansen and Doyle (1998).

To address this question, we need additional information and we turn to the TEM data acquired over the site. While governed by the same physical principles, each EM system senses the earth differently and may provide complementary information about the geometry and compo-

Table 3. The FEM 1D inversion parameters.

Data type	Bz (HCP) in-phase, quadrature		
Uncertainties	900 Hz	7200 Hz	56 kHz
	1 nT	3 nT	5 nT
Number of stations		1153	
Station spacing		15	
Line spacing		200 m	
Discretization	Depth		Cell size
	$0 < z < 40$ m		2.5 m
	$40 < z < 100$ m		5 m
	$1000 < z < 400$ m		10 m
Reference model		20 kΩm	

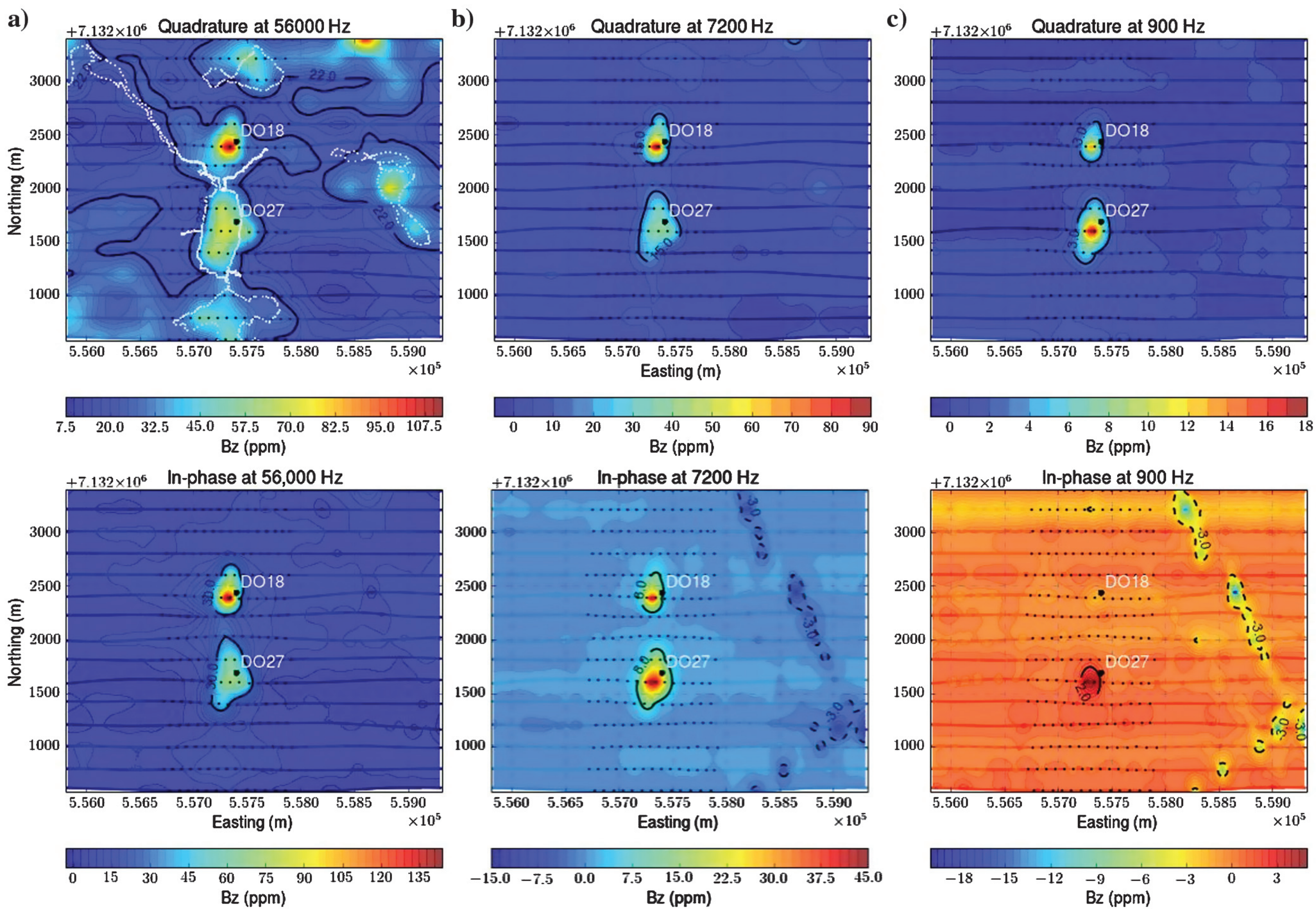

Figure 3. Coplanar in-phase and quadrature data at (a) 56,000 Hz, (b) 7200 Hz and (c) 900 Hz from the 1992 DIGHEM survey. Outlines of the hydrography (white) and flight lines (black) are shown for reference.

sition of the deposits. The expected depth of investigation of an EM system is a function of the skin depth δ_f and diffusion distance δ_t in the frequency and time domain, respectively (Ward and Hohmann, 1988):

$$\delta_f = \sqrt{\frac{\rho}{2\pi f \mu}}, \quad \delta_t = \sqrt{\frac{2\ t\rho}{\mu}}, \qquad (1)$$

where ρ is the resistivity (Ωm), f is the frequency (Hz), μ is the magnetic permeability (H/m), and t is the time (s). As a rule of thumb, higher frequencies and earlier time channels are sensitive to near-surface structures, whereas lower frequencies and later time channels are sensitive to deeper features.

TEM data

In the decade following the discovery of TKC, many airborne TEM surveys were undertaken to better characterize the deposits. Even though the FEM surveys were successful in identifying the two pipes, these surveys were not able to define a reliable vertical extent of the kimberlite pipes. In 1999, an AeroTEM I was flown (Boyko et al., 2001). Based on the conductive responses noted in the NanoTEM and FEM surveys, a strong positive EM response was expected over a broad range of time channels. Perplexingly, the earliest time channels recorded over DO-18 were negative; these negative responses were also observed over DO-27 on the late time channels. It was hypothesized that IP effects could be responsible for the negative responses (Smith and Klein, 1996), but these were early days for TEM systems. Subsequent AeroTEM II (2003) and VTEM (2004) surveys confirmed the negative responses over the two pipes (Jansen and Witherly, 2004) (Figures 6 and 7). Even though it was interesting from a scientific standpoint, extracting meaningful information from those negative data remained challenging at the time. This is still an area of active research (Kang and Oldenburg, 2015; Viezzoli et al., 2015; Macnae, 2016), and the processing and interpretation of airborne IP data will be addressed in the final study of this three-part series on TKC. For the remainder of this paper we shall work only with data that we feel are not severely contaminated with IP signals.

1D inversion

We had access to the AeroTEM II and VTEM surveys. Figure 8 compares typical decay curves measured by the AeroTEM and VTEM systems away from the main

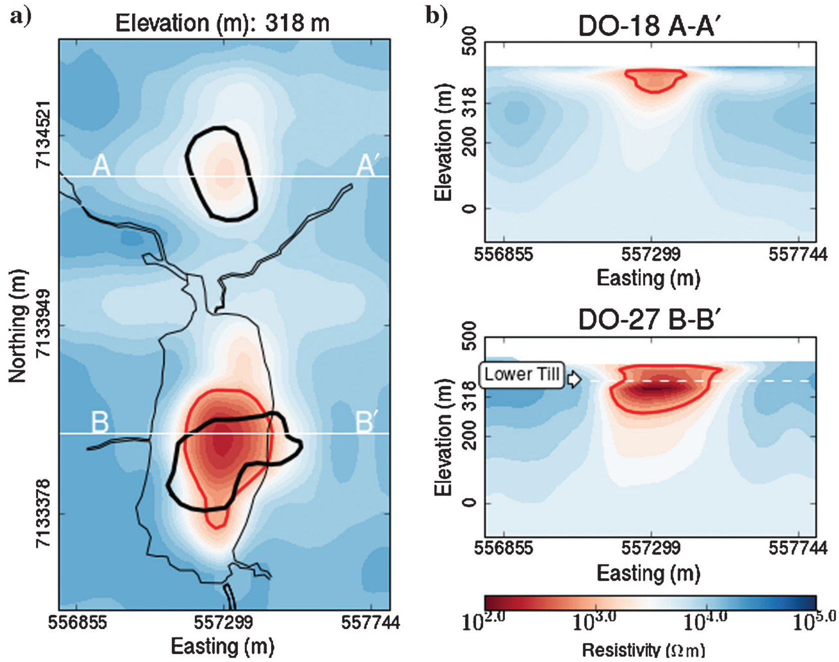

Figure 4. (a) Plan view and (b) vertical sections through the laterally constrained 1D conductivity model. Contour line for 1000 Ωm (red), outline of DO-18/DO-27 pipes (bold), and approximate depth of the till layer (white) are shown for reference.

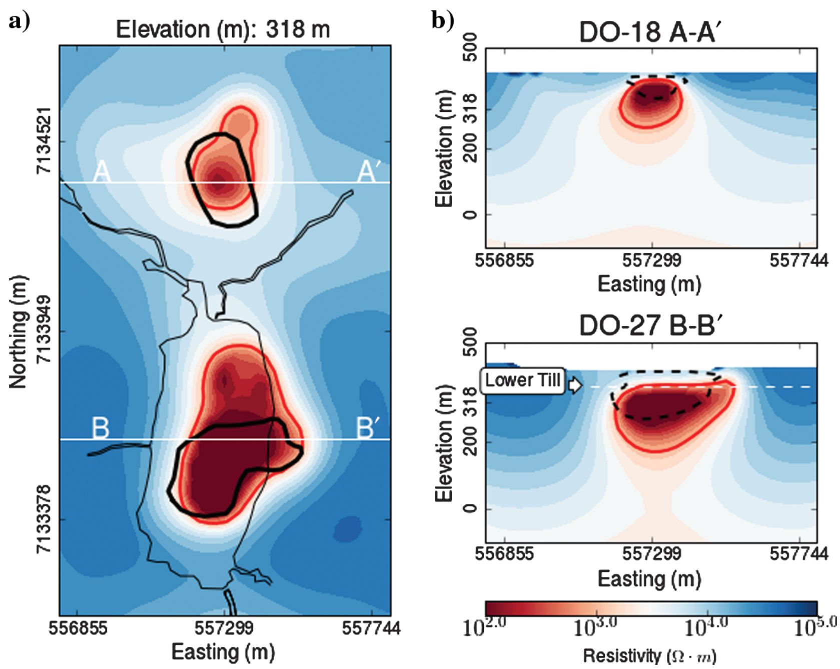

Figure 5. (a) Horizontal and (b) vertical sections through the 3D inverted conductivity model. Contour line for 1000 Ωm (red), outline of DO-18/DO-27 pipes (bold), and approximate depth of the till layer (white) are shown for reference. A contour line (dash) for 1000 Ωm obtained with the 1D inversion is shown for comparison.

EM anomalies. Note that the decay curves measured by the AeroTEM II are generally noisier. This trend is seen across the entire data set and for reasons that are unclear. As a result, we choose to only invert the positive VTEM data.

Using a similar strategy as implemented for the DIGHEM data, we first invert the VTEM data in one dimension with lateral constraints. Because few of the time channels measured over DO-18 are positive, we focus our efforts on DO-27. From the diffusion distance, it is expected that the TEM system would be sensitive to the deeper root of DO-27. We use the same mesh, starting conductivity, and inversion parameters as for the FEM 1D inversion. Figure 9 displays sections through the recovered conductivity model. The highest conductivity is centered at a depth corresponding to the interface between the till and the pipe below. The conductive anomaly extends to the surface and to depths of approximately 200 m. These features are generally consistent with the DIGHEM model previously shown in Figure 4.

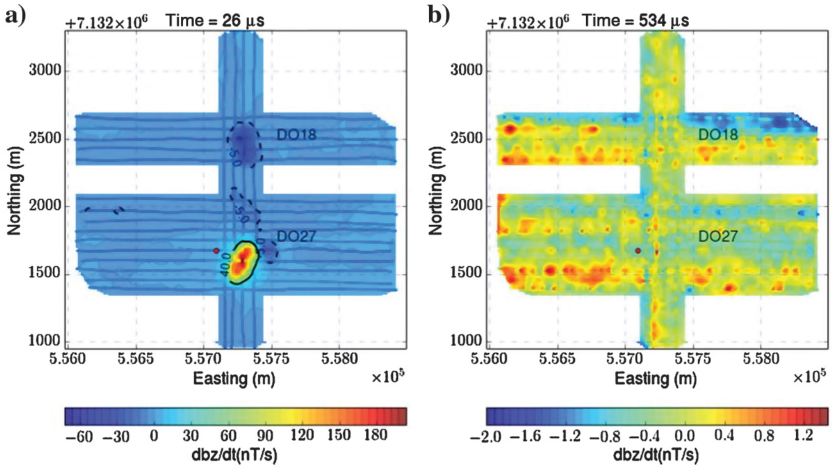

Figure 6. Observed data from the AeroTEM (2003) survey at (a) early and (b) late time channels.

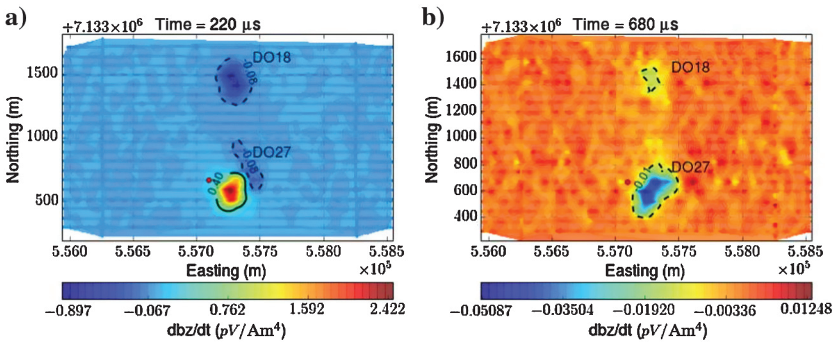

Figure 7. Observed data from the VTEM (2004) survey at (a) early and (b) late time channels.

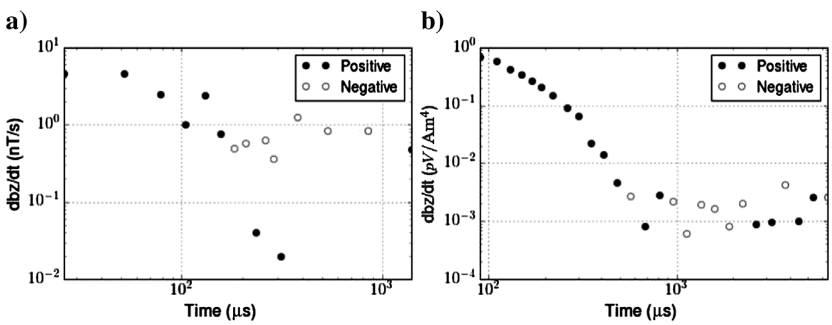

Figure 8. Comparative decay curve between the AeroTEM II (2003) and VTEM (2004) surveys away from the main EM anomalies.

To carry out the above analysis, we work only with positive data. It is, however, important to note that even the positive VTEM data at early times may still be contaminated with IP effects. Therefore, when trying to fit these decay curves in a voxel-based inversion code, these effects can manifest themselves as spurious artifacts, which may lead to erroneous interpretations. To minimize these artifacts, we turn to a parametric inversion method.

Parametric inversion

A parametric inversion differs from a voxel-based inversion in that instead of solving for the conductivity in every mesh cell, the inversion searches for a set of parameters that describes the conductivity distribution of interest. In this manner, only a few parameters are needed to define the spatial extent of the kimberlite pipe: the optimal background conductivity and the conductivity of the pipe itself. We have chosen a skewed Gaussian ellipsoid as the parameterization of choice. The algorithm only requires a generic starting guess for the location and conductivity of the kimberlite pipe. Further technical details of the parametric inversion method can be found in McMillan et al. (2015). Because the parametric inversion solves for only one anomaly with a well-defined shape, it prevents high-wavelength artifacts from entering the inversion. We perform the parametric inversion on the positive VTEM data, which corresponds to the first 10 time channels over DO-27. We ignore data over DO-18 and areas in between the two pipes where only negative data occur.

The starting guess for the parametric inversion is composed of a 1 Ωm, 150 m radius sphere positioned in the center of the positive DO-27 anomaly at a depth of 150 m. Upon completion, the inversion finds optimal conductivity values of 25 and 1040 Ωm for the pipe and background, respectively. Figure 10 compares the observed and predicted time-decay curves directly above DO-27. The fits are moderately good, but there is a systematic misfit with the predicted data having a lower amplitude at early times and a larger amplitude at later times compared with the field data. This may be a result of the simplistic parameterization or possibly due to the potential IP effects that were still in the data.

Sections through the recovered parametric model are presented in Figure 11a. The cross section shows the parametric model as a conductive bowl whose upper boundary is at the bottom of the lake. We assume that the lake water is too resistive and shallow to have a significant impact on the VTEM data. The general shape and location are similar to that obtained from the 3D FEM inversion.

Summary of independent inversions

We have so far inverted DIGHEM and VTEM data sets independently. While sensing the earth differently, both EM systems are probing the same conductivity structure and should therefore agree on the general shape of the kimberlite pipe. In both cases, the horizontal location and vertical extents of the DO-27 kimberlite pipe are consistent. The pipe appears to extend to depths greater than 200 m below the surface.

However, the two EM systems disagree on the upper limit of the pipe and on the absolute resistivity. The recovered 3D DIGHEM model suggests a distinct contrast at approximately 20–50 m below the lake bottom. This result seem to confirm that the main EM signal originated from the conductive pipe itself (≈100 Ωm) rather than the more resistive till layer and lake sediments (>1000 Ωm). From the 1D and parametric VTEM models, the anomaly extends directly from the bottom of the lake with a slightly lower resistivity value of 25 Ωm. These discrepancies can partially be attributed to the different parameterization used in the inversion, but there could be at least three fundamental explanations:

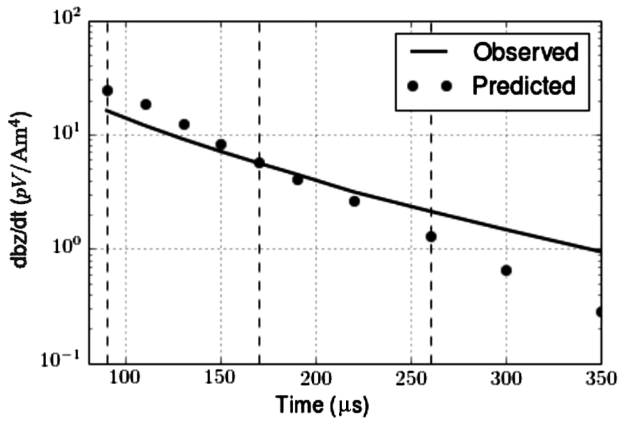

Figure 10. Observed and predicted decay curves from the parametric VTEM inversion as measured in the center of DO-27.

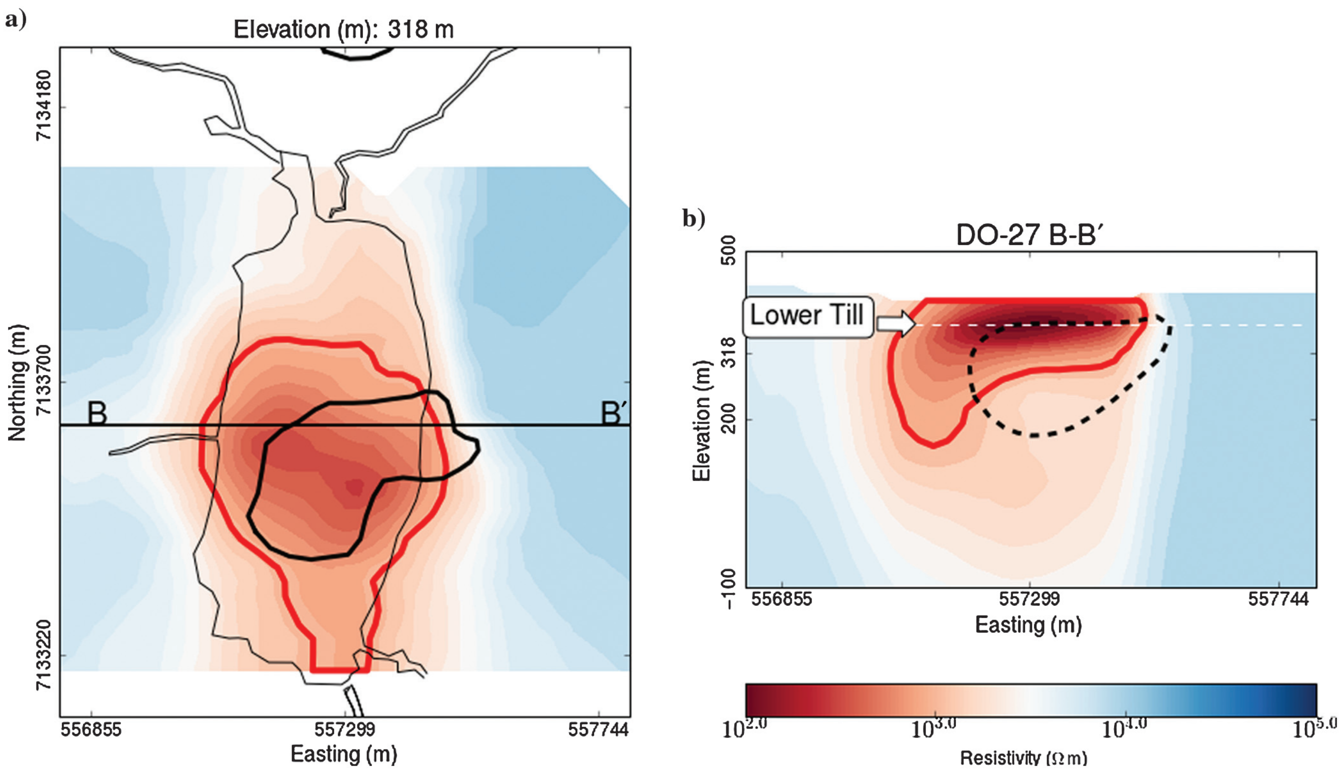

Figure 9. (a) Horizontal and (b) vertical sections through the VTEM 1D conductivity model. Contour line of approximately 1000 Ωm (red), outline of DO-18/DO-27 pipes (bold), and approximate depth of the till layer (white) are shown for reference. A contour line (dash) at approximately 1000 Ωm obtained with the 1D DIGHEM inversion is shown for comparison.

1) The skin depth for the highest DIGHEM frequency (56,000 Hz) is approximately 70 m, assuming 1000 Ωm resistivity within the pipe. This is much less than the diffusion distance of the earliest time (90 μs) of VTEM (≈400 m).Therefore, we expect a more accurate representation of the shallow structures from the DIGHEM survey.
2) The TKC complex is located within the Lac de Gras watershed, a sub-Arctic region with a documented permafrost layer of variable thickness (Golder Associated Ltd., 2014). Laboratory and field measurements have shown strong dependencies between the temperature and the EM response (Grimm and Stillman, 2015). There is a possibility that differences in absolute resistivity between the time and frequency-domain inversions are due to temperature because the surveys were flown at different times.
3) The temperature dependence of conductivity (Grimm and Stillman, 2015) and the presence of ice, as well as fine glaciofluvial sediments, can be the sources of significant IP signals. Although a time-domain inversion can be carried out with only positive data, we suspect that the earliest positive time channels are also impacted. The IP effects can also have an influence on the frequency-domain data. We have assumed that the IP contamination in the frequency-domain data was small enough to be ignored, but that may contribute to the discrepancies.

Thus, we have two data sets, one in frequency and the other in time, that are possibly affected by temperature and IP effects to an unknown degree. However, these variables are difficult to quantify without in situ measurements and remain a source of uncertainties in our study. Nevertheless, in our quest for finding the best conductivity model to characterize TKC, we use a cooperative inversion approach.

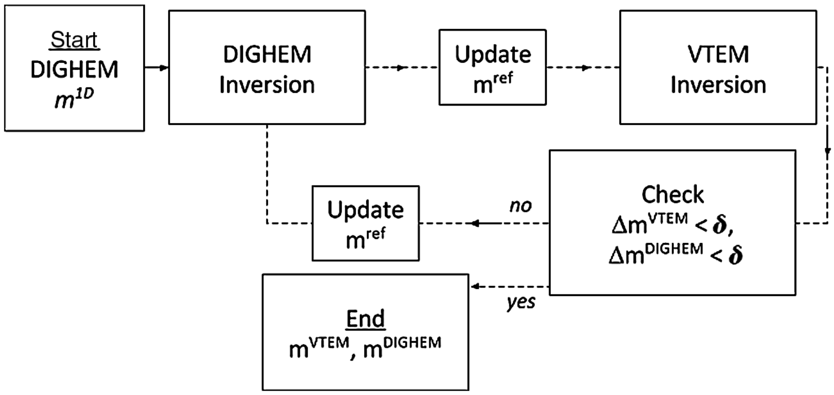

Figure 12. Cooperative inversion workflow.

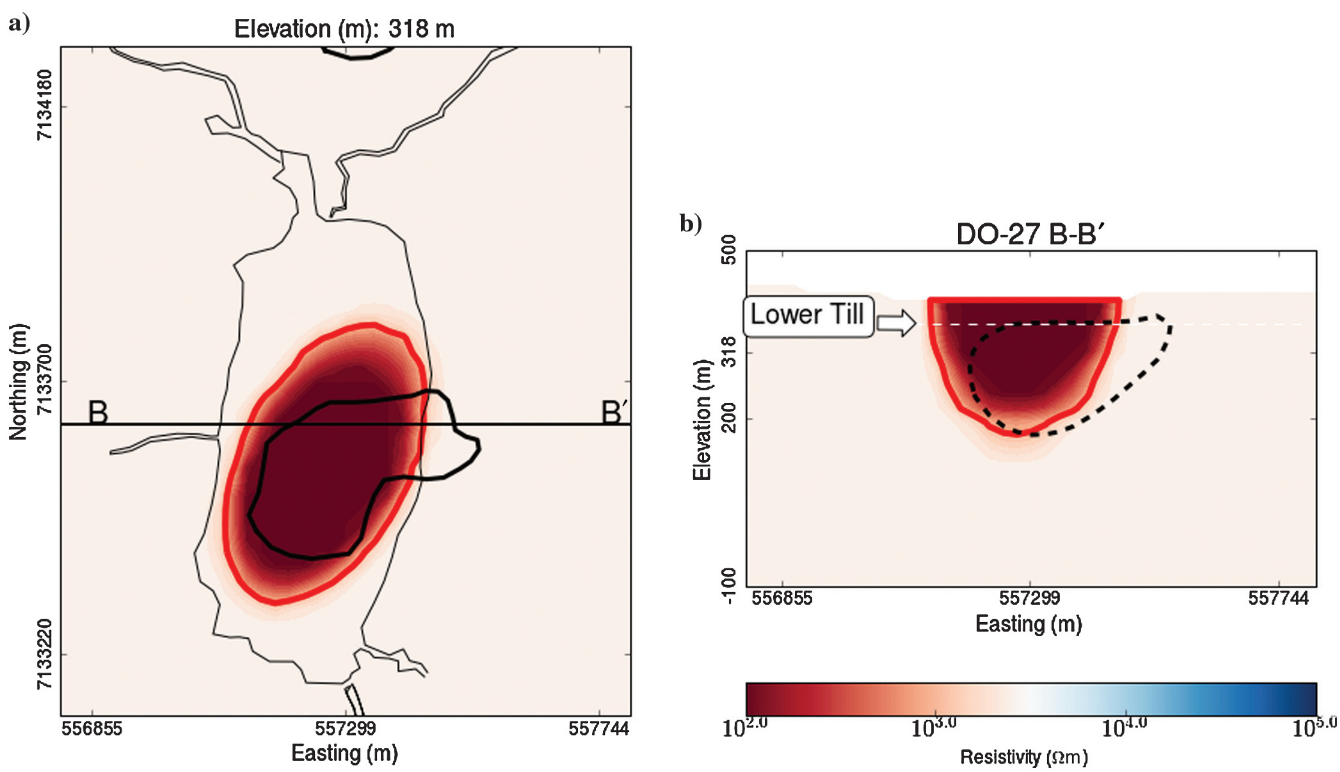

Figure 11. (a) Horizontal and (b) vertical sections through the parametric conductivity model. Contour line for 1000 Ωm (red), outline of DO-18/DO-27 pipes (bold), and approximate depth of the till layer (white) are shown for reference. A contour line (dash) at approximately 1000 Ωm obtained with the 3D DIGHEM inversion is shown for comparison.

Cooperative EM inversion

To find a conductivity structure that adequately explains the deposits, we reinvert both data sets with a cooperative inversion strategy (McMillan and Oldenburg, 2014). Due to the limited coverage of the positive VTEM data, we limit the analysis to DO-27. Figure 12 shows a schematic representation of the cooperative inversion workflow. First, the DIGHEM data are inverted in one dimension to get a general distribution and range of conductivity values. Because this model is already stored and interpolated in three dimensions, it is readily transferred to a different mesh to serve as a starting model for the 3D code. The outcome of the 3D DIGHEM inversion is then used as a reference model to guide the VTEM inversion. This iterative process is repeated until (1) both data sets can be predicted within an acceptable level and (2) the recovered models do not change substantially between each cycle ($\Delta \mathbf{m} < \delta$). Four iterations were required in our case.

Figure 13 compares the sequence of inverted models, starting from the unconstrained 1D model to the final cooperative models. The cooperative method has been successful in greatly reducing the discrepancy between the inversion results from the two EM data sets. Nevertheless, there are differences. Although the shape of the conductor is the same in both images, the VTEM inversion shows a shallower pipe with higher conductivity, than does the final DIGHEM model. There are many potential reasons why we are not able to further reduce discrepancies, including normalizations and processing of individual data sets, IP and temperature effects, and inversion parameters used in separate algorithms. For the remaining analysis in this paper, we will use the final DIGHEM model because it provides full coverage over the entire TKC area, and, as discussed earlier, we have more confidence in its near-surface resolving capabilities. However, the final VTEM model will be used for the processing of the IP data in our third and final paper (Kang et al., 2017).

Analysis

Conductivity is an important physical property to help delineate the kimberlite pipe from the host rocks and surface sediments. Figure 14 presents a close-up section over the conductivity anomaly recovered over DO-27, overlaid with the thickness of the till layer obtained from the published drilling results (Eggleston

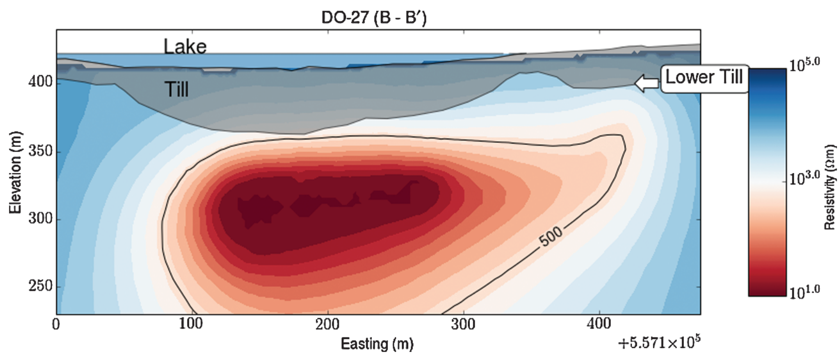

Figure 14. Near-surface conductivity model over DO-27 obtained from the cooperative inversion.

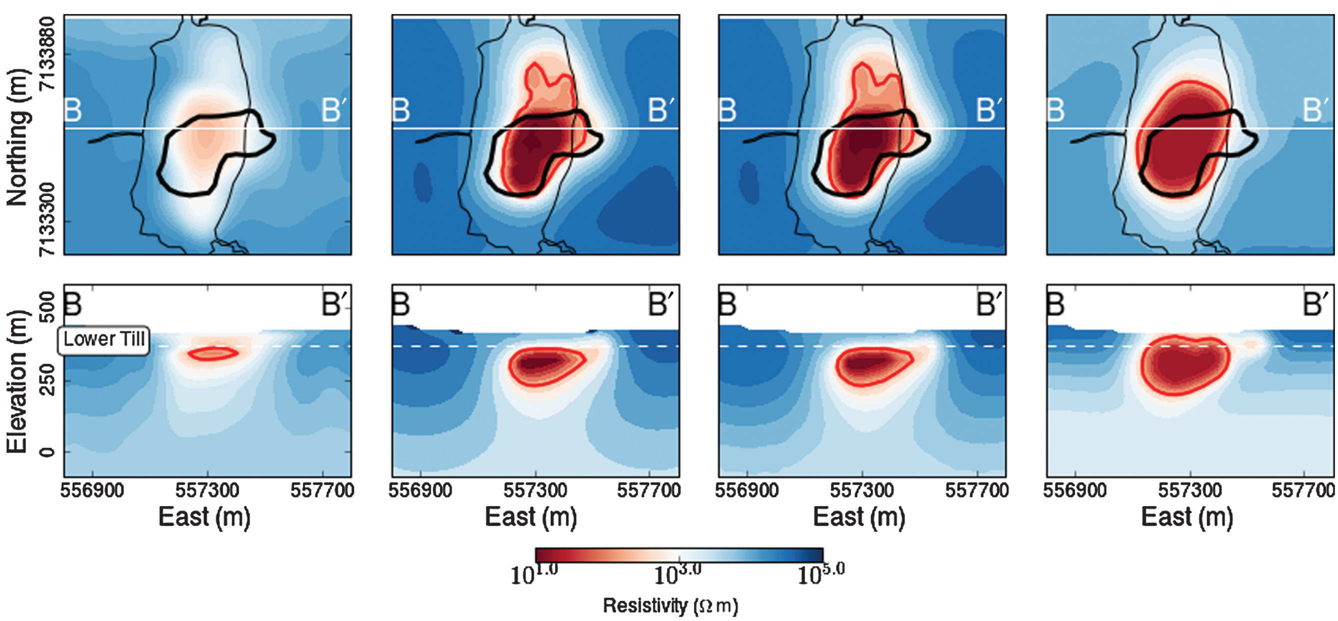

Figure 13. Comparative sections though the conductivity models from the (a) unconstrained FEM 1D inversion, (b) unconstrained FEM 3D inversion, (c) final cooperative FEM, and (d) final cooperative TEM model. A contour line at approximately 500 Ωm (black dash), the outline of the hydrography (black), and the approximate depth of the till layer over DO-27 (white dash) are shown for reference.

Table 4. Petrophysical domains built from inversions.

	Rock unit	Density contrast	Susceptibility	Conductivity	Rock type
	R0	High	Low	Low	Host
	R1	Low	Low-moderate	Low	Unclassified
	R2	Low	Low-moderate	High	PK/VK
	R3	Low-moderate	High	Low	HK

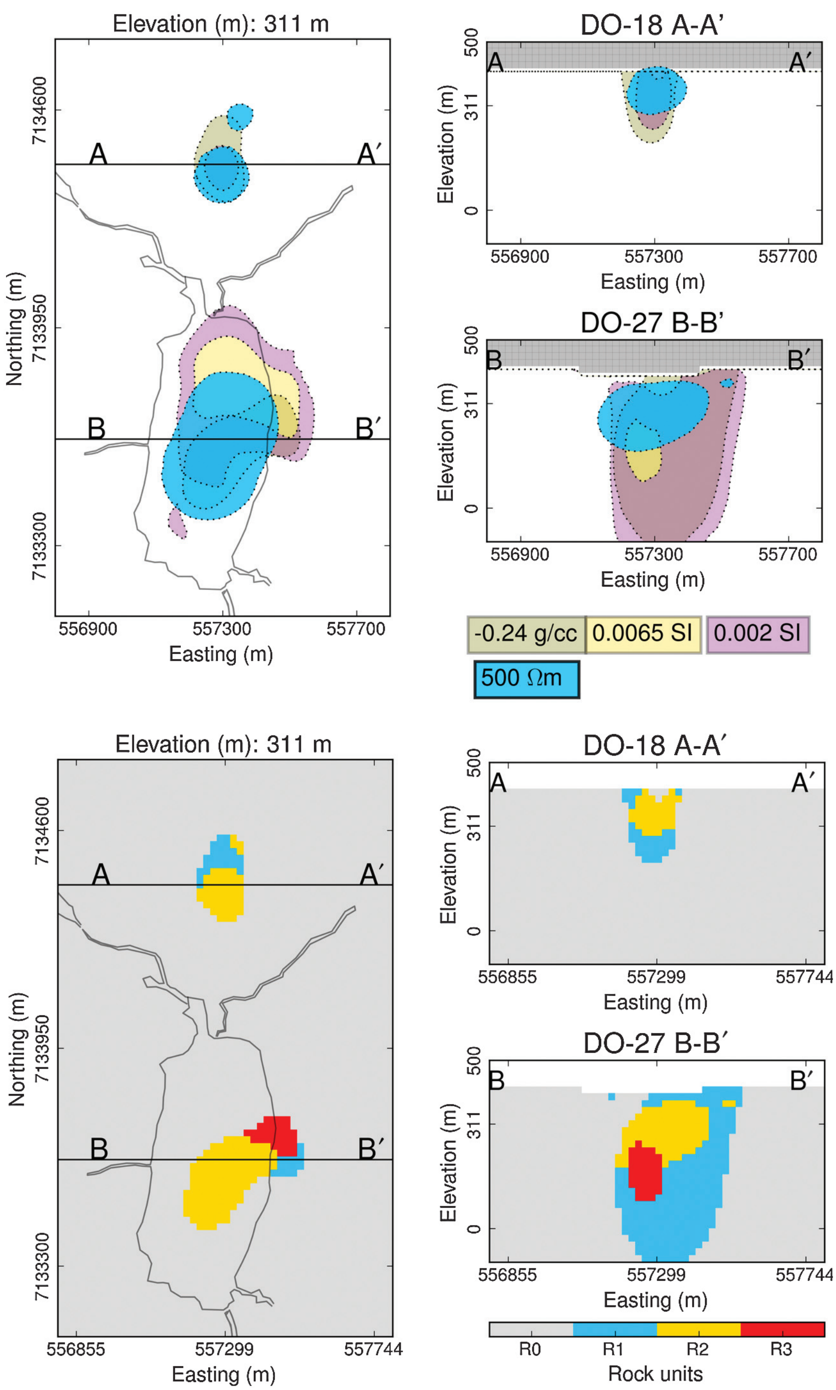

Figure 15. (a) Comparative sections through the density, susceptibility, and conductivity model using cutoff values and (b) petrophysical model built from the union of anomalous physical properties.

and Brisebois, 2008). The final conductivity model answers some of the original questions about the conductivity distribution:

1) The flat and broad conductive layers observed in previous 1D studies are likely due to 3D artifacts.
2) The main EM response appears to come from the kimberlite itself rather than from the till layer or lake bottom sediments, but the highest conductivity seems to be limited to the upper region of the pipes.
3) The DIGHEM system has the sensitivity to characterize the top of DO-27, but it is unlikely that it can be used to image the deeper root with confidence as postulated by others. The complementary VTEM survey increases our depth resolution. Both data sets agree on a response coming from the upper 150 m of the kimberlite pipe and below 50 m of sediments.

Ideally, we would like to characterize DO-18 and DO-27 based on the recovered resistivity values. Both pipes are modeled as low-resistivity anomalies in the order of 100 Ωm, which may suggest that they are similar in composition. However, it is important to note that the presence of a lake above DO-27 may insulate the ground from freezing, which in turn affects the frequency response. Because temperature can influence the recovered resistivity to an unknown degree, we cannot confidently differentiate the rocks making up DO-18 and DO-27 based on EM methods alone.

Petrophysical model

In the first paper (Devriese et al., 2017) of a three-part series on TKC, our colleagues characterize the kimberlite pipes from gravity and magnetic data. They build a preliminary rock model based on the 3D distribution of density and magnetic susceptibility and identify at least three rock units (R0–R2) as summarized in Table 4. From the density contrast, the outline of both pipes is easily distinguishable from the background Archean granitic rocks (R0), whereas the magnetic data subdivide the kimberlite rocks into regions of low-moderate (R1) and high (R3) susceptibility. The R3 unit was inferred to be an hypabyssal kimberlite (HK) unit limited to the northern region of DO-27. Low-to-moderate susceptibility was recovered over DO-18 and in the southern part of DO-27, known to be pyroclastic in nature (XVK, VK, and PK). From a potential field standpoint, the rocks making up the core region of both pipes can hardly be distinguished.

In this research, we recovered a final conductivity model from the cooperative inversion of two airborne EM systems. We wish to integrate these results to obtain an enhanced geologic description of the TKC deposits strictly from airborne geophysics. Building upon our previous analysis, we overlay anomalous values of density, susceptibility, and conductivity from our 3D models as shown in Figure 15a. Low-resistivity anomalies (<1000 Ωm) correlate well with the density lows, mainly in defining a clear interface at 20–40 m depths over DO-27, whereas DO-18 outcrops at the surface.

Using the union of the different physical property contrasts, we are able to build the updated petrophysical model presented in Figure 15b. After adding conductivity, we distinguish a fourth rock unit (R2) limited to the upper portion of DO-18 and DO-27. This unit reaches close to the surface at DO-18 but limits the upper boundary of DO-27 to approximately 50 m below the topography. The added resistivity information also highlights a strong contrast between the R3 unit and the core region of DO-27 and DO-18. Even though R3 had been identified as a high magnetic anomaly, it also has a much higher resistivity. This result increases our confidence that R3 be associated with the hypabyssal HK unit.

With the addition of the fourth rock unit, there appears to be a distinction between the upper and lower portions of DO-27 and DO-18. We had previously identified these volumes as an R1 unit. The open question is whether the DIGHEM and VTEM systems are insensitive to the deeper root of the pipe, or if resistivity increases at depth. The latter would support the idea of highly weathered kimberlite rocks with vertical variations in alteration, comparable with vertical gradation observed in the density (Eggleston and Brisebois, 2008). More work needs to done to confirm whether this is the case.

This simple analysis illustrates how airborne geophysics could have helped better define the various rock units at TKC, had these methods been available at the early stage of exploration. Our petrophysical model was derived entirely from three independent geophysical experiments and their respective inversions. No information regarding the known geology has been used to constrain the inversion. Yet, we have recovered a pseudogeologic model with reasonably accurate estimates of the location and the extent of DO-18 and DO-27 kimberlite pipes.

Conclusion

The recovered resistivity model obtained from a cooperative inversion of DIGHEM and VTEM data over TKC suggests that the EM anomalies originate from the kimberlite pipes, with only minor contributions from the till layer and the lake bottom sediments.

The conductivity model also helps to constrain the volume and upper extent of both pipes. The conductive DO-18 pipe appears to be shallower than DO-27, which agrees well with the known geology.

The combination of susceptibility and conductivity information refines our understanding about DO-27. The magnetic data highlighted a region in the northern portion of the pipe. This corresponds to a region of moderate resistivity, and we identify this as an HK unit. The core of DO-27 has high conductivity, and this coincides with a volume of low-to-intermediate susceptibility. We identify this volume as being a different kimberlitic rock, either PK or VK, but we cannot differentiate between them. Both rocks are similar in composition and are mainly distinguished by their crystal size and texture.

Even though IP effects are often regarded as noise in the airborne EM data, they may contain valuable information about the kimberlite deposits. In the third and final papers, we will use the conductivity models developed here to show how additional information can be extracted from the VTEM data to further characterize different kimberlite units at TKC.

Acknowledgments

The authors would like to thank K. Witherly and J. Jansen for the stimulating discussions about the TKC data sets during the past 15 years and for identifying the challenges for inverting and interpreting these data. We also thank J. Pell, B. Clements, B. Doyle, T. Arvanis, and R. Enkin for discussions about the data and geologic interpretations. We especially thank Condor Consulting Inc., Peregrine Diamonds, and Kennecott for making the data sets available for our research. Finally, we are indebted to other UBC-GIF members for their efforts on this two-year project: S. Devriese, K. Davis, D. Bild-Enkin, N. Corcoran, D. Cowan, L. Heagy, D. Marchant, L. A. C. Mata, M. Mitchell, and D. Yang.

Appendix A

Laterally constrained 1D inversion

The standard 1D inversion framework considers each sounding as an independent experiment. Several factors including variations in the noise level and 1D assumptions for 3D objects can introduce rapid changes in conductivity between neighboring soundings. LCI has been proposed by Auken and Christiansen (2004) to smooth the result along the survey line. The procedure has been adapted in 3D by Viezzoli et al. (2008), called spatially constrained inversion (SCI), creating smoothness across survey lines. Both methods use a measure of lateral roughness to penalize horizontal variations in conductivity. The SCI method has been borrowed by other researchers in geophysics (Steuer et al., 2008; Santos et al., 2011). Here, we incorporate a hybrid strategy using EM1DFM inversion algorithm as our central solver (Farquharson et al., 2003). The main difference with the SCI method is that each sounding is still inverted independently, avoiding the need to form a large linear system of equations. Between each 1D iteration, an average conductivity model is interpolated onto a global 3D mesh

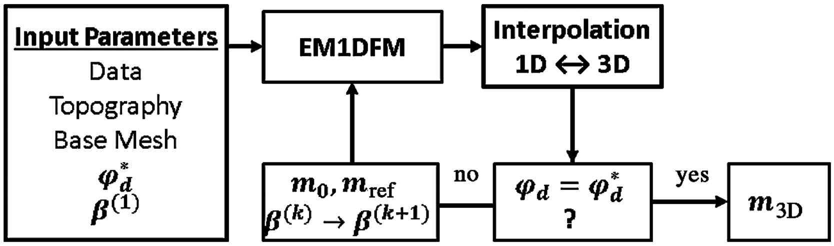

Figure A-1. Laterally constrained 1D inversion workflow.

and used as a reference for subsequent inversions. A global data misfit and regularization parameters are used to control individual 1D inversions, similar to the framework used for 3D algorithms. Figure A-1 presents the algorithm workflow.

References

Auken, E., and A. V. Christiansen, 2004, Layered and laterally constrained 2D inversion of resistivity data: Geophysics, **69**, 752–761, doi: 10.1190/1.1759461.

Boyko, W., N. R. Paterson, and K. Kwan, 2001, AeroTEM: System characteristics and field results: The Leading Edge, **20**, 1130–1138, doi: 10.1190/1.1487244.

Devriese, S. G. R., K. Davis, and D. W. Oldenburg, 2017, Inversion of airborne geophysics over the DO-27/DO-18 kimberlites — Part 1: Potential fields: Interpretation, **5**, this issue, doi: 10.1190/int-2016-0142.1.

Eggleston, T., and K. Brisebois, 2008, DO-27 Diamond Project, Northwest Territories: Ni 43-101 report, AMEC.

Farquharson, C. G., D. W. Oldenburg, and P. S. Routh, 2003, Simultaneous 1D inversion of loop-loop electromagnetic data for magnetic susceptibility and electrical conductivity: Geophysics, **68**, 1857–1869, doi: 10.1190/1.1635038.

Golder Associated Ltd., 2014, Permafrost baseline report for the Jay Project: Technical report, Dominion Diamond Ekati Corporation.

Grimm, R. E., and D. E. Stillman, 2015, Field test of detection and characterisation of subsurface ice using broadband spectral-induced polarisation: Permafrost and Periglacial Processes, **26**, 28–38, doi: 10.1002/ppp.v26.1.

Haber, E., and C. Schwarzbach, 2014, Parallel inversion of large-scale airborne time-domain electromagnetic data with multiple OcTree meshes: Inverse Problems, **30**, 055011–055028, doi: 10.1088/0266-5611/30/5/055011.

Jansen, J., and K. Witherly, 2004, The Tli Kwi Cho kimberlite complex, Northwest Territories, Canada: A geophysical case study: 74th Annual International Meeting, SEG, Expanded Abstracts, 1147–1150.

Jansen, J. C., and B. J. Doyle, 1998, The Tli kwi Cho kimberlite complex, Northwest Territories, Canada: A geophysical post mortem: Presented at the NWMA Practical geophysics short course, Northwest Mining Association.

Kang, S., D. Fournier, and D. W. Oldenburg, 2017, Inversion of airborne geophysics over the DO-27/DO-18 kimberlites — Part 3: Induced polarization: Interpretation, **5**, this issue, doi: 10.1190/int-2016-0141.1.

Kang, S., and D. W. Oldenburg, 2015, Recovering IP information in airborne time domain electromagnetic data: Presented at the 24th International Geophysical Conference and Exhibition.

Macnae, J., 2016, Quantitative estimation of intrinsic induced polarization and superparamagnetic parameters from airborne electromagnetic data: Geophysics, **81**, no. 6, E433–E446, doi: 10.1190/geo2016-0110.1.

Masun, K. M., 1999, The petrography and mineralogy of the Lac de Gras kimberlite field, Slave Province, Northwest Territories: A comparative study: Master of science, Department of Geology, Lakehead University.

McMillan, M. S., and D. W. Oldenburg, 2014, Cooperative constrained inversion of multiple electromagnetic data sets: Geophysics, **79**, no. 4, B173–B185, doi: 10.1190/geo2014-0029.1.

McMillan, M. S., C. Schwarzbach, E. Haber, and D. W. Oldenburg, 2015, 3D parametric hybrid inversion of time-domain airborne electromagnetic data: Geophysics, **80**, no. 6, K25–K36, doi: 10.1190/geo2015-0141.1.

Power, M., and D. Hildes, 2007, Geophysical strategies for kimberlite exploration in northern Canada: Proceedings of Exploration 2007: 5th Decennial International Conference on Mineral Exploration, 1025–1031.

Santos, F. A. M., J. Triantafilis, and K. Bruzgulis, 2011, Case History: A spatially constrained 1D inversion algorithm for quasi-3D conductivity imaging: Application to DUALEM-421 data collected in a riverine plain: Geophysics, **76**, no. 2, B43–B53, doi: 10.1190/1.3537834.

Smith, R. S., and J. Klein, 1996, A special circumstance of airborne induced-polarization measurements: Geophysics, **61**, 66–73, doi: 10.1190/1.1443957.

Steuer, A., B. Siemon, and A. Viezzoli, 2008, Application of spatially constrained inversion on HEM and Skytem data: Presented at the 5th International Conference on Airborne Electromagnetics.

Viezzoli, A., A. V. Christiensen, and E. Auken, 2008, Quasi-3D modeling of airborne TEM data by spatially constrained inversion: Geophysics, **73**, no. 3, F105–F113, doi: 10.1190/1.2895521.

Viezzoli, A., V. Kaminski, Y. L. Cooper, L. Hardy, and G. Fiandaca, 2015, Improving modelling of AEM data affected by IP, two case studies: 24th International Geophysical Conference and Exhibition, CSEG, Extended Abstracts, 1–5.

Ward, S. H., and G. W. Hohmann, 1988, Electromagnetic theory for geophysical applications: SEG, Investigation in Geophysics 1, 130–311.

Witherly, K., 2005, Report on VTEM test program over three kimberlite, Lac de Gras area, Northwest Territories: Technical report, Condor Consulting.

Yang, D., and D. W. Oldenburg, 2014, 3D inversion of airborne electromagnetic data parallelized and accelerated by local mesh and adaptive soundings: Geophysical Journal International, **196**, 1492–1507, doi: 10.1093/gji/ggt465.

Biographies and photographs of the authors are not available.